

Network Formation and Dynamics Among Multi-LLMs

MARIOS PAPACHRISTOU, Cornell University, USA

YUAN YUAN, Purdue University, USA

Social networks shape opinions, behaviors, and information dissemination in human societies. As large language models (LLMs) increasingly integrate into social and professional environments, understanding their behavior within the context of social interactions and networks becomes essential. Our study analyzes LLMs' network formation behavior to examine whether the dynamics of multiple LLMs are similar to or different from human social dynamics. We observe that LLMs exhibit key social network principles, including preferential attachment, triadic closure, homophily, community structure, and the small-world phenomenon, when asked about their preferences in network formation. We also investigate LLMs' decision-making based on real-world networks, revealing that triadic closure and homophily have a stronger influence than preferential attachment and that LLMs perform well in network formation predictions. Overall, our study opens up new possibilities for using LLMs in network science research and helps develop socially aware LLMs by shedding light on their network formation behaviors and exploring their impacts on social dynamics.

Additional Key Words and Phrases: large language models, networks, network formation, link prediction, multi-agent systems

1 INTRODUCTION

Recent progress in large language models (LLMs), such as GPT [39] and LLaMA2 [47], have shown promising developments in AI techniques and their integration into real-life applications. It is thus crucial to comprehend AI actions to ensure they align with human expectations, mitigate potential risks, and maximize their benefits. Misaligned AI actions may lead to unintended consequences, such as biased decision-making, fairness issues, and the miscoordinative or non-cooperative behavior [45]. Recently, researchers have started to apply methodologies, such as methods analogous to laboratory experiments [1, 22, 32, 50], agent-based modeling [16, 17, 19, 21, 43, 44], and qualitative methods, to study LLMs. These methods help uncover the generative capabilities of LLMs and their interpretability [12, 22, 28, 42].

In human societies, social networks play a crucial role in shaping individual behaviors, preferences, and connections, as well as influencing the diffusion of information and norms across communities [3, 4, 18, 46, 53]. LLMs have shown great potential in social contexts, notably as intelligent personal assistants facilitating social and business interactions (see, e.g., [13, 41, 50]). However, less is known about how LLMs' innate behaviors and preferences align with human network formation principles [23, 42, 54]. This is particularly crucial, as it sheds light on the potential of these models to shape and be shaped by the intricate networks of human relationships, which is a fundamental aspect of social systems.

Our study thus explores LLMs' behaviors and preferences in network formation in both synthetic and real-world social networks. By analyzing interactions between multiple LLMs (or multi-LLMs), we aim to understand the implications of LLMs representing humans in social and business settings. Specifically, we examine micro-level social network properties including preferential attachment [6], triadic closure [20], and homophily [34], as well as macro-level properties including community structure [38], and the small-world phenomenon [26, 52].

In synthetic networks, our findings reveal that LLMs can generate networks exhibiting preferential attachment and following scale-free degree distributions. Moreover, LLMs demonstrate strong tendencies toward triadic closure and exhibit tendency of homophily. These tendencies further explain the emergence of community structures with high modularity in networks formed by multiple LLMs. Additionally, we show that LLM agents exhibit dynamics consistent with small-world phenomena akin to those observed in the Watts-Strogatz model [52].

ALGORITHM 1: Prompt used to implement $Q(A_t, i_t, \delta)$ formatted as a Python f-string.

```

# Task
Your task is to select a set of people to be friends with.

# Profile
Your profile is given below after chevrons:
<PROFILE>F({i_t})</PROFILE>

# Candidate Profiles
The candidate profiles to be friends with are given below after chevrons:

<PROFILES>F(A_t)</PROFILES>

# Output
The output should be given a list of JSON objects with the following structure

[
  {{
    "name" : name of the person you selected,
    "reason" : reason for selecting the person
  }}, ...
]

# Notes
- The output must be a list of JSON objects ranked in the order of preference.
- You can make at most  $\delta$  selections.

```

Next, we conduct a comparative analysis of these principles to identify the key factors driving network dynamics in the context of real-world network formation scenarios. To do so, we consider real-world networks and ask each LLM to simulate a node in the network. We provide information on their network structure and ask for their decisions for the next link formation or dissolution step. We approach this problem as a discrete choice modeling problem [29, 40]. In this real-world setting, we find that LLMs’ choices are primarily weighted on homophily and triadic closure, compared to preferential attachment, and that LLMs substantially exceed random guessing when predicting new links. Additionally, the resulting choices of LLM agents strengthen the network’s community structure.

Our study contributes to the literature on LLMs in several ways. First, it advances the discussion on aligning LLMs with human social preferences, which has potential applications in developing socially aware LLMs for real-life interactions. Insights into LLMs’ innate behaviors in network formation can inform the design of LLMs for effective collaboration in social and professional settings. Second, our work has direct applications to synthetic dataset generation, a problem important for the graph learning community. By controlling for a few parameters, such as the temperature, our work can be utilized to generate a variety of datasets, as well as generate synthetic datasets from real-world data to protect privacy. Finally, our study could contribute to understanding the impact of LLMs on social dynamics and norms, such as their role in shaping online communities’ interaction patterns or influencing the adoption of new communication norms in professional settings.

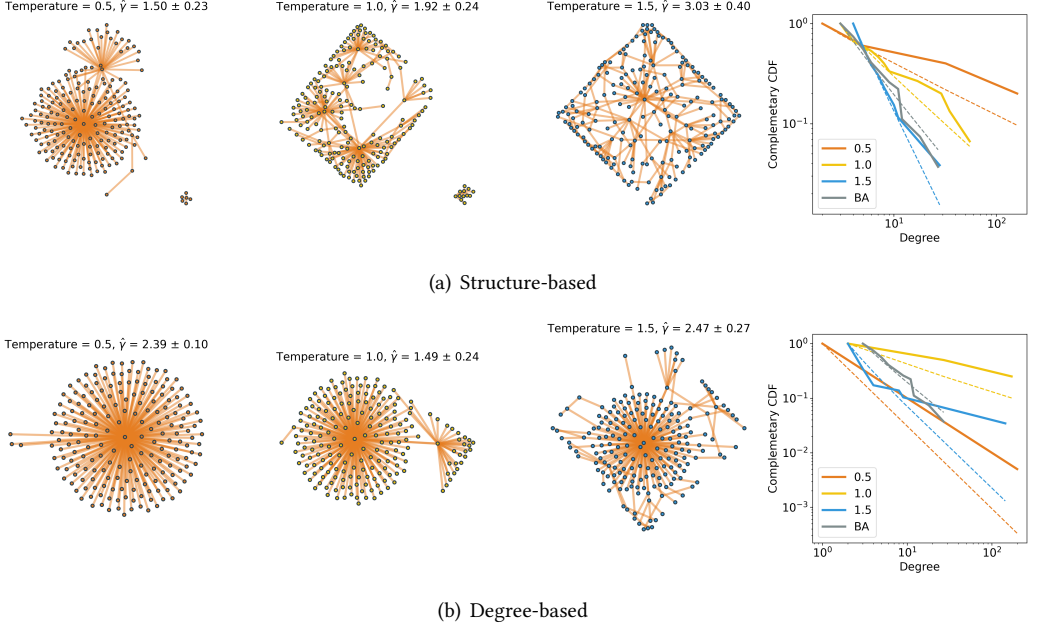


Fig. 1. Networks with $n = 200$ nodes created based on Principle 1 for various temperatures. For the structure-based networks (Figure 1(a)), we provide the multi-LLMs with the neighborhoods $\{N_{j,t} : j \in i_t\}$, and for the degree-based networks (Figure 1(b)), we provide the degrees $\{d_{j,t} : j \in i_t\}$ of the nodes $j \in i_t$. We also plot the degree distribution and compare it against a BA network with $n = 200$ nodes. **Top:** In Figure 1(a), we observe that the resulting networks follow a power-law degree distribution ($P > 0.5$, Bootstrap hypothesis test). When the temperature is 1.5, the resulting network resembles the BA model ($P < 0.001$, K-S test). **Bottom:** When the degree information is provided only (Figure 1(b)), the resulting networks correspond to unrealistic star-like formations that are far from a scale-free network and resemble more a core-periphery network.

2 RESULTS

Our study employs the state-of-the-art LLMs, such as GPT-3.5 and GPT-4 [39] with the OpenAI API¹. We constructed multiple LLMs using multiple independent conservation threads where each thread represents one multi-LLM. We prompt each LLM by providing information about other LLMs' network information as well as decisions they are faced with. We test both state-of-the-art GPT-based models: for the results of Sections 2.1 and 2.2, we use GPT-3.5 agents, and in Section 2.3, we use GPT-4 agents. We obtained similar results using GPT-3.5 and GPT-4. Overall, we adopted a standard framework for multi-LLMs but underscored the multi-agent nature of the design in our setting [1, 2, 11, 16, 28]. We evaluate the robustness of our results by testing various temperature settings in LLMs, which control the degree of variation of the model output. All experiments employ a dynamic network setup. We also employ an interview-like approach to inquire about the rationale behind the decisions of LLMs. The details of our methods are presented in *Methods*.

In this section, we first discuss three major micro-level network principles: preferential attachment, triadic closure, and homophily. We then examine two macro-level network principles:

¹For GPT-3.5 we use the gpt-3.5-turbo model provided by OpenAI, and for GPT-4 we use the gpt-4-1106-preview model.

community structure and small-world phenomenon. Subsequently, we test the strength of these principles when LLM agents face real-world networks and compare the preferences in network formation tasks between LLMs and humans.

2.1 Micro-Level Properties

Principle 1: Preferential Attachment. Preferential attachment is a well-known mechanism in network science that explains how certain nodes in a network become more connected over time, leading to the emergence of highly connected vertices and scale-free distribution of degree [6, 7].

We examine whether LLMs exhibit the preferential attachment mechanism in the following way: First, we start with an empty network and add nodes at each time step t . For each new time step, we add a new node i_t , providing information on the network neighbors of all existing nodes.² We chose to generate networks with $n = 200$ nodes, as this size is sufficiently large to allow for the observation of degree distribution patterns.

We plot one of the examples of resulting networks under each temperature in Figure 1(a). As observed in all temperature setups, we observe a few nodes that have many connections, and the majority of the nodes have one or few connections, which renders the degree distribution scale-free, i.e., the probability $\pi(d)$ a node has degree d is given by

$$\pi(d) \propto d^{-\gamma}, \quad \text{where } \gamma > 1.$$

Furthermore, we observe more “super nodes” with many connections as the temperature increases.

We also compare with the Barabási–Albert (BA) model [6] where each incoming node t , the probability $p_{i,t}$ of it connecting to node i is proportional to $d_{i,t}$, where $d_{i,t}$ is the degree of node i at time step t , namely,

$$p_{i,t} = \frac{d_{i,t}}{\sum_{j=1}^t d_{j,t}}.$$

For temperatures of 0.5 and 1.0, we find that the estimated exponent values are $\hat{\gamma} = 1.50 \pm 0.23$ and 1.92 ± 0.24 , respectively. However, the degree distributions do not resemble the degree distribution of the generated BA network with an expected exponent $\gamma = 3$. This is supported by the P -values from a two-sample Kolmogorov–Smirnov (K-S) test, which are $P < 0.001$ and $P < 0.05$, respectively when compared to the empirical degree distribution of the BA network³.

Moreover, for all temperatures, the resulting degree distribution is scale-free ($P > 0.5$, bootstrapping hypothesis test comparing with the fitted scale-free distribution).

We also examine the network formation when only degree information (rather than network structure) is provided, in a similar spirit of [16]. We present the results in Figure 1(b). We observe “star-like” formations around one node. The degree distributions differ from scale-free distributions produced by statistical models such as the BA model ($P < 0.001$, two-sample K-S test compared to the empirical distribution of the generated BA network). They are closer to a core-periphery network [10].

Finally, we employ text analysis of reasoning provided by the agents for the results of Figure 1(a)⁴. We observe two main categories of reasons (see Appendix C) for the fraction under each temperature):

²See Appendix E, for information about how the features are represented in the prompt.

³As shown by [5], the BA model follows a scale-free distribution of the form $\pi_{\text{BA}}(d) \propto d^{-3}$ for sufficiently large n . However, because our n is small, so that the prompt does not exceed the token limit for the GPT-3.5 model, we directly compared it to a sample from the BA model (the generated network has $\hat{\gamma}_{\text{BA}} = 2.24 \pm 0.24$), instead of comparing with the limiting distribution $\pi_{\text{BA}}(d)$.

⁴We do not provide the distribution of reasons for the results of Figure 1(b) as all of the LLM’s decisions are made given the degree information.

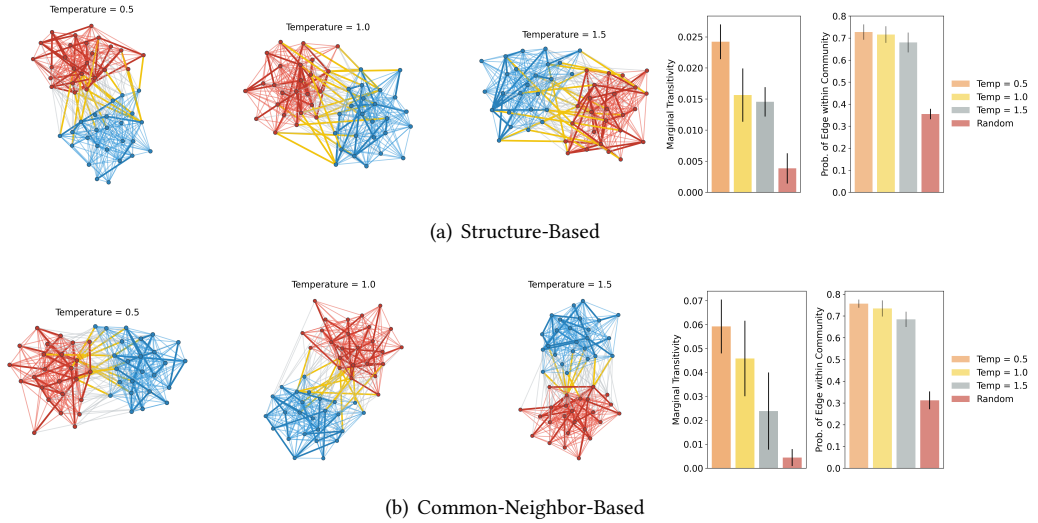


Fig. 2. Networks created based on Principle 2. **Top:** Figure 2(a) shows the resulting networks created by Principle 2 when the intersection of the neighborhoods of the query node and each alternative is provided. The node colors correspond to the stochastic block model (SBM) groups each node belongs to. The red edges correspond to the newly created edges between nodes of the red cluster, the blue edges correspond to the newly created edges between nodes of the blue cluster, and the orange edges correspond to edges created between the two clusters. The newly formed edges are drawn with a larger line width. We observe that the probability of forming an edge within the same community and the marginal transitivity, which indicate triadic closure, is significantly larger than randomly creating links ($P < 0.001$, t-test). **Bottom:** Figure 2(b) shows the same networks with the only change that instead of the intersection of neighborhoods between the query node and each alternative, we provide the number of common neighbors (i.e., the size of the intersection) between the query node and each alternative. Similarly, we observe that the probability of forming an edge within the same community and the marginal transitivity, which indicate triadic closure, is significantly larger than randomly creating links ($P < 0.001$, t-test).

- *Well-Connectedness*: it corresponds to reasons related to the person being well-connected and having many friends.
- *Mutual Friends*: it is related to having many friends in common with the person so that the person can introduce them to their friends.

The well-connectedness reason becomes less prevalent as the temperature increases, and the mutual friends' reason becomes more prevalent. Note that when the temperature is 1.5, the two reasons have almost the same frequency.

Taken together, networks created by LLM systems, when given a network structure, demonstrate preferential attachment and exhibit scale-free degree distributions.

Principle 2: Triadic Closure. The second micro-level principle we examine is triadic closure, which describes the phenomenon that individuals are likely to form connections with their friends' friends, leading to closed triads within the network. This tendency enhances the network's structure and cohesion, rooted in the likelihood of two nodes forming a direct connection if they share a common neighbor [20, 35].

To test for triadic closure, we use an assortative stochastic block model (SBM) [36] to generate an initial seed network G_1 with n nodes divided into two equal-sized clusters A and B . Connections

within each cluster have a probability of 0.5, while connections across clusters have a probability of 0.1. This setup reflects our intuition that nodes within the same cluster are more likely to form connections due to their higher number of common neighbors. We then iterate over each node i , providing features based on the intersection of the neighborhoods of all of i 's non-neighbors or the number of common friends between i and any non-neighbor j . This modeling choice contrasts the results mentioned about preferential attachment, where the neighborhood information is provided and made to make the two settings consistent⁵.

We compare this with the random null model, which selects a node at random to connect to. We run ten simulations for $n = 50$ nodes.⁶

To measure whether the principle of triadic closure exists, we employ the *fraction \hat{p} of newly added edges between nodes of the same community*, i.e., the fraction of edges in $G_T \setminus G_1$ that have their ends both at either A or B , namely

$$\hat{p} = \frac{|\{\{i, j\} \in E(G_T) \setminus E(G_1) : y_i = y_j\}|}{|E(G_T) \setminus E(G_1)|},$$

where $y_i, y_j \in \{A, B\}$ are the community memberships of nodes i and j respectively, and $E(G_T) \setminus E(G_1)$ corresponds to the newly added edges.

Generally, a value of $\hat{p} > 0.5$ indicates the tendency of triadic closure since an LLM agent, which is supposed to exhibit triadic closure given the common neighbors, would ideally create a link within the same cluster.

Additionally, we introduce the concept of *marginal transitivity* for the network, represented by D . This metric is defined as the change in the proportion of closed triangles to open triads in the network, from G_T (the initial network) to G_1 (which corresponds to the SBM):

$$D = 3 \times \frac{\# \text{triangles}(G_T)}{\# \text{triads}(G_T)} - 3 \times \frac{\# \text{triangles}(G_1)}{\# \text{triads}(G_1)}.$$

We depict the sample outcomes in Figure 2(a), where the upper panel presents the results when the entire network structure is provided, whereas the lower panel only provides the number of common neighbors. Node colors correspond to their respective groups within the SBM. Red edges denote connections within the red cluster, blue edges within the blue cluster, and orange edges between the two clusters. Newly established edges are emphasized with a thicker line width.

We present the probabilities of network formation within a community in the last panels in each row. We find that the probability of forming a within-community tie across all temperatures is substantially larger than the random network formation scenario ($P < 0.001$, t-test comparing to Random), suggesting LLMs' tendency of triadic closure (since an LLM which is given the common neighbors as features should ideally create links within the same community).

Additionally, we observe a statistically significant increase in the marginal transitivity D for all temperatures ($P < 0.001$, t-test). Moreover, in all cases, the marginal transitivity D is statistically significant compared to Random ($P < 0.001$, t-test).

⁵We want to note that performing the same experiment when we provide the neighbors instead of the common neighbors produces similar results.

⁶For better visualization, we chose $n = 50$ nodes instead of a large number of nodes such as $n = 200$. Moreover, the results are statistically significant even with $n = 50$ nodes.

These results suggest that LLM agents exhibit the tendency of triadic closure. Similar to the approach in earlier reasoning analysis, we present the most common reasons provided by LLMs in Appendix C⁷. We find that most of the agents base their decisions on the number of mutual friends.

Principle 3: Homophily. Homophily reflects the tendency for nodes with similar characteristics or attributes to form connections and associate with each other. This phenomenon is based on the principle that individuals in a network are more likely to connect with others who share similar traits, interests, or demographics [34].

To test whether LLM agents exhibit homophily, we perform the following experiment: We generate nodes with randomly generated attributes regarding a hobby (randomly chosen among three hobbies), a favorite color (randomly chosen among three colors), and a location within the US (randomly chosen among three US locations) and provide the attributes of the other nodes and the node’s own attributes, and each node is tasked to form up to $\delta = 5$ links with others. For each node i , we provide it with the features x_j of all non-neighbors j of i . The seed network is taken to be the empty graph.

We run ten simulations for networks with $n = 50$ nodes and $\delta = 5$. We compare with the Random null model, which chooses $\delta = 5$ links at random.

To measure the presence of homophily, we measure the attribute assortativity coefficient of each of the three features (hobby, color, location). For a property P which takes K distinct values P_1, \dots, P_K , its *assortativity coefficient* R is defined as

$$R = \frac{\sum_{i=1}^n M_{ii} - \sum_{i=1}^n a_i b_i}{1 - \sum_{i=1}^n a_i b_i},$$

where M is the mixing matrix with entries M_{ij} corresponding to the fraction of edges where one end has value P_i , and the other end has value P_j , $a_i = \sum_{j=1}^n M_{ij}$ and $b_i = \sum_{j=1}^n M_{ji}$. The assortativity has values between -1 and $+1$, where a positive value denotes the tendency of the nodes to connect to other similar nodes (hence yielding a homophilous network), and a negative value corresponds to connecting to the tendency to connect to dissimilar nodes (which indicates heterophily).

In Figure 3, we observe a consistent pattern of positive assortativity across all temperature ranges, which is higher for lower temperatures. Moreover, the observed assortativity at all temperatures significantly deviates from Random, which has assortativity close to 0 ($P < 0.001$, t-test comparing with Random). Taken together, we conclude homophily emerges for the networks generated by LLMs.

Moreover, we present the probability of each reason being mentioned in Appendix C. We find that shared hobbies appear to be much more important than shared location or favorite color. This is consistent with our intuition that, similarly to humans, LLMs care more about hobbies than other superficial attributes when forming social connections.

2.2 Macro-Level Principles

Principle 4: Community Structure. The community structure of networks refers to the organization of nodes or individuals within a network into distinct and densely interconnected groups or clusters [8, 15, 37, 38]. Identifying community structures is crucial for understanding the overall dynamics of a network, as it reveals patterns of relationships and interactions that might not be apparent at the global level.

⁷We do not provide the distribution of reasons for the results of Figure 2(b) as all of the LLM’s decisions are made given the number of common neighbors information.

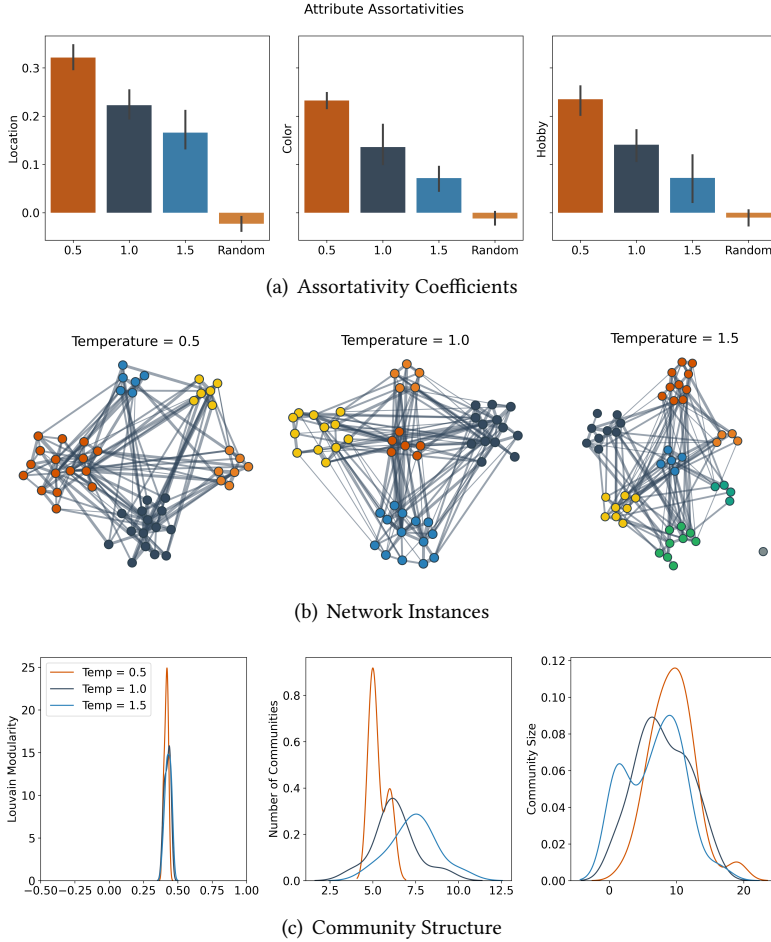


Fig. 3. **Top:** Figure 3(a) shows the assortativity coefficients for each network attribute created based on Principle 3. Each node can form at most $\delta = 5$ links with the other nodes based on their attributes. We observe that for all temperatures, we have positive assortativity ($P < 0.001$, t-test with 0), which indicates homophily. The assortativities are significantly different for all temperatures from random or heterophilous ($P < 0.001$, t-test comparing with Random) **Middle:** Networks created based on Principle 3. Each node can form at most $\delta = 5$ links with the other nodes based on their attributes. The edge widths correspond to the number of common attributes shared between the nodes. We report the probability of forming a link as a function of the number of common attributes between two nodes. The node colors correspond to the communities found by running the Louvain algorithm. **Bottom:** Louvain modularity, number of communities, and community sizes of networks created based on Principle 3. Lower temperatures yield higher modularity ($P < 0.001$, t-test) and fewer and larger communities ($P < 0.001$, t-test). For smaller temperatures, the communities are more “well-separated”.

Both triadic closure and homophily contribute to the formation of community structures. By examining how these two factors contribute to network formation, we aim to gain insights into the underlying mechanisms driving community dynamics in LLM-generated networks. We employ the

simulation results presented in Section 2.1 to determine whether community structure in networks generated by LLMs emerges from triadic closure or homophily.

First, we consider the networks generated in Figure 2. We examine how LLM agents’ choices strengthen the network’s community structure. Specifically, we leverage the fact that the SBM graph has a preexisting community structure and measure how the newly formed links reinforce such a structure. Visual inspection shows that the newly added links, represented by the bold edges, happen mostly within each cluster, reinforcing the community structure. This is further quantitatively verified by the fraction \hat{p} newly created inter-community edges. We find that \hat{p} is significantly higher than 0.5 ($P < 0.001$, t-test comparing with 0.5). This indicates that most edges are within the same community, strengthening the community structure.

Next, we use modularity maximization [8] to examine the community structure that arises due to homophily. Intuitively, the modularity measure compares the number of edges inside a community with the expected number of edges that one would find in the cluster if the network were a random network with the same number of nodes and where each node keeps its weighted degree, but edges are otherwise randomly attached according to the Chung-Lu model [14]. This random null model implicitly assumes that each node can attach to another network node. Formally, for a graph with weights w_{ij} on its edges, the *weighted modularity* Q [15] of a partition with C communities given by

$$Q = \sum_{c=1}^C \left[\frac{L_c}{W} - r \left(\frac{k_c}{2W} \right)^2 \right],$$

Here W is the sum of all weights, L_c is the total weight of intra-community links for community c , k_c is the total weighted degree of the nodes in the community c and r is the resolution parameter which (we take $r = 1$ from now on). A large positive value (such as greater than 0.5) of the modularity corresponds to evidence of community structure, corresponding to deviation from the random null model. Maximizing Q is NP-Hard, we use the Louvain algorithm [8] to get a lower bound on the maximum modularity.

In Figure 3(b), we illustrate the communities identified by the Louvain algorithm at various temperatures. Alongside, we present the average Louvain modularity values over ten simulations, with 95% confidence intervals (refer to Figure 3(c)). For the network’s weights, we use the number of common attributes shared between each pair of nodes. This is defined as $w_{ij} = \left| \left\{ k : x_i^{(k)} = x_j^{(k)} \right\} \right|$ for each link (i, j) in the final network. Here, $x_i^{(k)}$ and $x_j^{(k)}$ correspond to the k -th features of x_i and x_j , respectively.

We observe that the Louvain partitions demonstrate community structure with positive modularity across all temperatures. This is confirmed by a t-test comparing the modularity to $Q = 0$ of a random graph ($P < 0.001$). The modularity is most pronounced at lower temperatures. As the temperature increases, the Louvain modularity also increases ($P < 0.001$, t-test). Furthermore, lower temperatures result in fewer (and larger) communities on average, as identified by the Louvain algorithm ($P < 0.001$, t-test). Additionally, communities tend to be visually more distinct at lower temperatures. We propose that higher temperatures reflect increased randomness in the decisions.

Our results demonstrate that community structures manifest in networks generated by LLMs. Specifically, these networks adhere to the principle of triadic closure, which further reinforces the formation of community structures. Additionally, LLM-generated networks exhibit homophily, facilitating the emergence of distinct communities. In Section 2.3, we further illustrate that community structures are reinforced in real-world networks, where LLMs consider a combination of factors, including homophily and triadic closure, in their decisions to form connections.

Principle 5: Small-World. The small-world phenomenon is characterized by networks where nodes are interconnected in tight clusters, yet the average distance between any two nodes remains relatively short, typically scaling logarithmically with the network size [26, 52]. This balance between high clustering and short path lengths characterizes small-world networks.

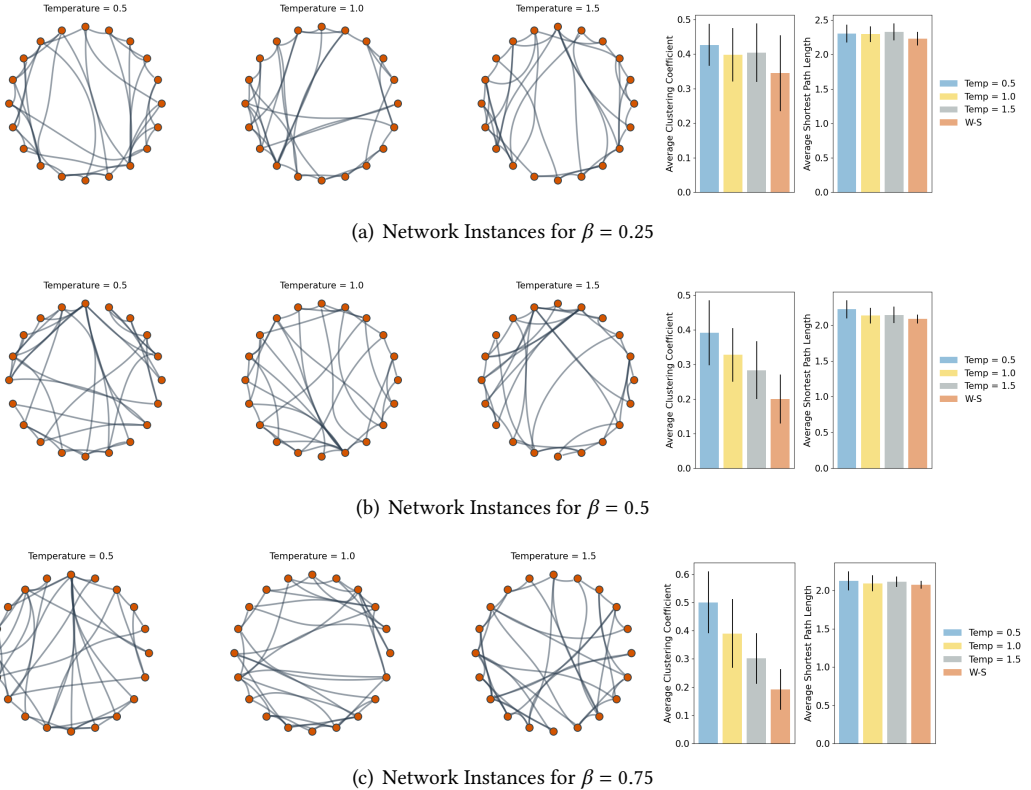
Formally, a small-world network is a network where the *average shortest path length* L grows proportionally to the network size n ,⁸ namely

$$L \sim \log(n).$$

Our analysis utilizes the Watts-Strogatz model [52] as a benchmark to investigate whether LLMs can generate networks exhibiting small-world characteristics. This model has a delicate balance between local clustering and short average path lengths: Nodes tend to form clusters or groups (triadic closure), exhibiting a high level of interconnectedness within these local neighborhoods, whereas at the same time, the existence of a few long-range connections ensures that the entire network is reachable with relatively few steps [25, 31, 43].

We employ a modified version of the model, where edge rewiring is informed by LLM queries, based on the current network structure. The generation process is parametrized by the number of nodes (n), the number of long-range connections (k), and the rewiring probability (β). The algorithm proceeds as follows:

⁸This follows the definition in [24].



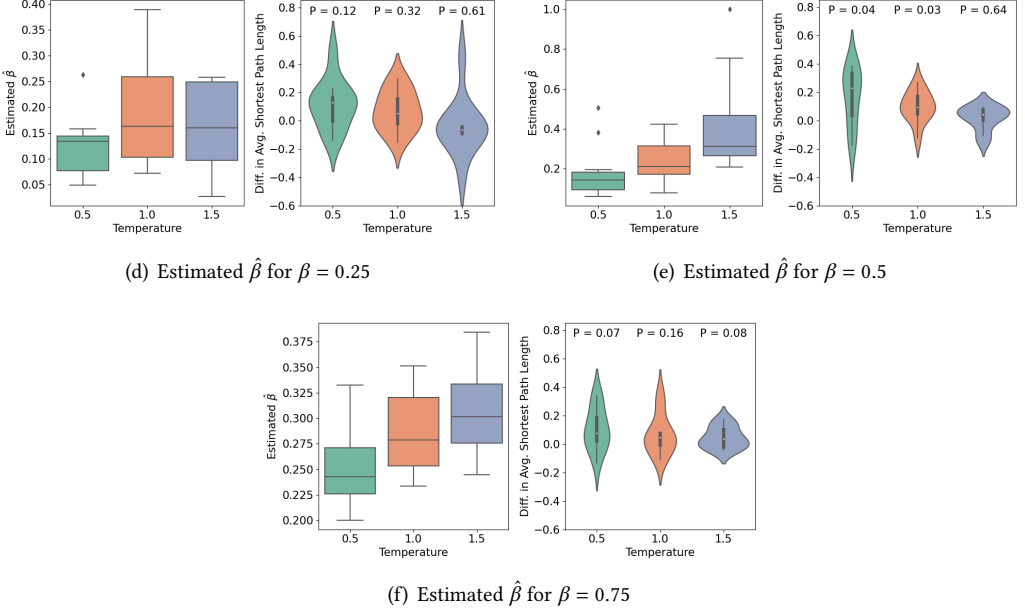


Fig. 3. **Figures 4(a) to 4(c):** and distribution of reasoning created based on Principle 5 using the altered Watts-Strogatz Model for $n = 50, k = 5, \beta \in \{0.25, 0.5, 0.75\}$, together with plots of the average clustering coefficient C and the average shortest path length L . The comparison is made with respect to a Watts-Strogatz graph with $n = 50, k = 5, \beta \in \{0.25, 0.5, 0.75\}$. In most cases, we observe strong evidence that $L \sim \log(n)$ and $C \sim 1/\log(n)$. **Figures 4(d) to 4(f):** Estimated values $\hat{\beta}$ of $\beta \in \{0.25, 0.5, 0.75\}$ for LLM-generated networks based on matching the average clustering coefficient and difference in the average shortest path between LLM-generated networks and Watts-Strogatz with rewiring probability $\hat{\beta}$. We report the P -values of the t-test comparing the average shortest path length of the LLM-generated networks and the average shortest path length of the Watts-Strogatz graphs with rewiring probability $\hat{\beta}$.

- (1) Similarly to Watts-Strogatz, we first create a ring network with n nodes. After that, for each node $[n]$, we create k edges where $k/2$ edges connect to its rightmost neighbors and $k/2$ edges connect to its leftmost neighbors.
- (2) To create G_t , for each node $[n]$, we take its $k/2$ rightmost neighbors and rewire them with probability β . For each of the $k/2$ rightmost neighbors that are to be rewired, we make one query to the LLM, which indicates how the edge will be rewired. The choice is made by providing the LLM with all the network nodes and each node's neighbors (i.e., the network structure).

The model closely resembles the Watts-Strogatz model, with the primary distinction being the method of edge rewiring. Instead of randomly selecting edges for rewiring, as in the Watts-Strogatz model, we determine the rewiring of an edge by inquiring about the LLM and providing it with the current network structure.

We generate networks with varying sizes ($n = 10$ to $n = 100$) and examine the relationships between the average shortest path length (L) and the average clustering coefficient (C) with respect to the network size (n). We test $\beta \in \{0.25, 0.5, 0.75\}$ and set $k = 5$ as an illustration. In addition, we compare with the results reported in [24]. Some instances of these networks are shown in Figures 4(a) to 4(c). We run regressions relating to the average shortest path length with $\log(n)$

and observe that for all temperatures, we obtain statistically significant results (see the significance indicators in Figure 4, where most regressions have $P < 0.001$) being that the average shortest path length scales proportionally to $\log(n)$. Similarly, we show that the average clustering coefficient scales as $1/\log(n)$ (again, most regression results have $P < 0.001$). Both results follow the guideline from [24] which tested the small-world properties of organizational networks.

However, a direct comparison with the Watts-Strogatz model reveals that the LLM-generated networks do not exactly mirror the statistics of Watts-Strogatz networks with corresponding β values. As Figures 4(a) to 4(c) show, we only observe weak evidence that the final generated networks have a similar average shortest path length as Watts-Strogatz with $\beta \in \{0.25, 0.5, 0.75\}$ ($P < 0.1$, t-test comparing the resulting average shortest path lengths of the networks generated by multi-LLMs and the Watts-Strogatz average shortest path lengths for $\beta \in \{0.25, 0.5, 0.75\}$) and a larger average clustering coefficient than Watts-Strogatz ($P < 0.1$, t-test comparing the resulting average clustering coefficient of the networks generated by multi-LLMs and the Watts-Strogatz average clustering coefficient for $\beta \in \{0.25, 0.5, 0.75\}$).

To quantify this resemblance, we conduct a binary search to identify the $\hat{\beta}$ values for which the Watts-Strogatz networks’ average clustering coefficients match those of the LLM-generated networks. The results, depicted in Figures 4(d) to 4(f), show that while the average shortest path lengths are not identical, they are sufficiently close, with the differences not being statistically significant at the 0.1 level for most temperature settings. In Figures 4(d) to 4(f), we plot the estimated values for $\hat{\beta}$ for each value of β , each simulation and each temperature together with the P -values resulting from a t-test comparing with the average shortest path length of Watts-Strogatz with rewiring probability $\hat{\beta}$.

In conclusion, our analysis demonstrates that LLM-generated networks exhibit key small-world properties, with logarithmic scaling of average shortest path lengths and inverse logarithmic scaling of average clustering coefficients. While these networks do not perfectly align with the Watts-Strogatz model, they exhibit similar structural characteristics, underscoring the potential of LLMs in generating small-world networks.

2.3 Real-World Networks

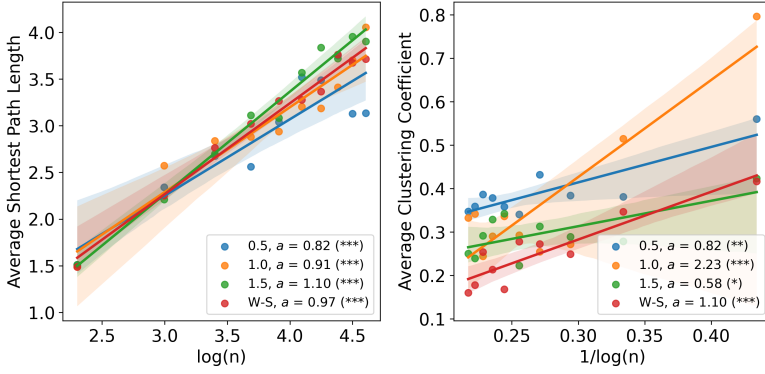
To investigate the behavior of LLMs in real-world network formation contexts, we employ the *Facebook100* dataset [49] and a discrete choice modeling framework [33, 40]. This dataset comprises “friendship” networks from one hundred American colleges and universities, captured at a specific moment in time from Facebook’s online social network. We model the network formation process as a discrete choice process, wherein nodes are sequentially prompted to form connections from a set of available alternatives.

2.3.1 Discrete Choice Model. For each node i_t that we consider at time t , we randomly remove one of its current friends from the real-world network. After we remove a neighbor for each of i_1, \dots, i_T , we end up with the network G_1 , which we use as a seed network for the LLM agents.

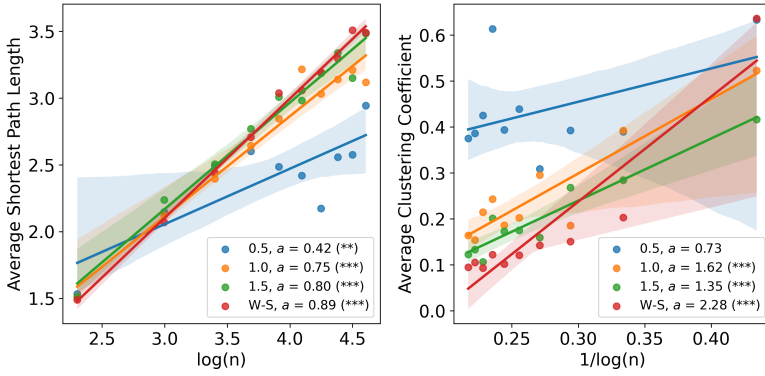
Subsequently, during the link formation process, we present each node i_t with a set of candidate nodes (denoted by A_t), comprising one of the previously removed friends and other nodes that are not their friends. We then instruct the LLM to form a link with one of the candidates, providing the attributes of the candidates and the social network structure to aid its decision-making. These choices are made sequentially.

We use the *utility* of the model for each node for each sequential decision of network formation:

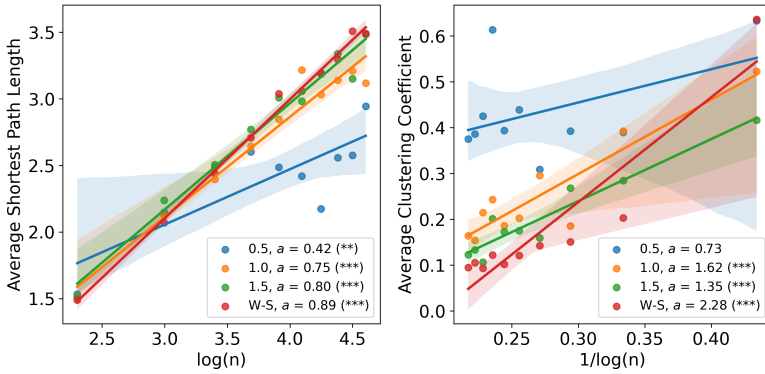
$$U_{ij,t} = \theta_{PA} \log d_{j,t} + \theta_H \log w_{ij} + \theta_{TC} \log c_{ij,t} + \epsilon_{ij,t}.$$



(g) $\beta = 0.25$



(h) $\beta = 0.5$



(i) $\beta = 0.75$

Fig. 4. Regression plots relating average shortest path length and average clustering coefficient with n for $\beta \in \{0.25, 0.5, 0.75\}$ and $k = 5$. a represents the slope of the regression lines. * indicates $P < 0.05$, ** indicates $P < 0.01$, and *** indicates $P < 0.001$.

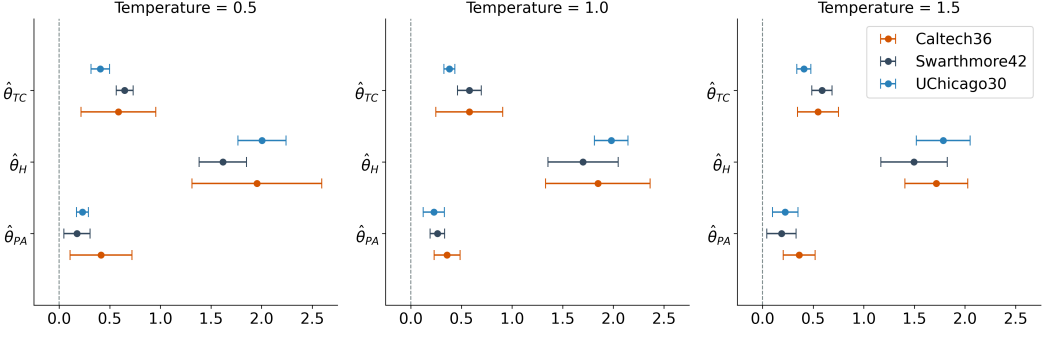


Fig. 5. Multinomial logit coefficients for three networks from the Facebook100 dataset. The standard errors of the estimates are shown with error bars. The full regression tables can be found in Appendix A. All coefficients are statistically significant, where the null hypothesis corresponds to the respective parameter being equal to 0.

In this equation, θ_{PA} measures the strength of preferential attachment based on the degree $d_{j,t}$ of j at step t , θ_H measures the strength of homophily based on the similarity w_{ij} (i.e. number of common attributes) between i and j , and θ_{TC} measures the strength of triadic closure, based on the number of common neighbors $c_{ij,t}$ between i and j at step t . The error term $\epsilon_{ij,t}$ is distributed as i.i.d. standard Gumbel⁹. All variables are first normalized based on their range, and then the log transformation is taken.

The multinomial logit model (MNL) indicates that the probability that i links to j at step t is given by

$$p_{ij,t} = \Pr [\operatorname{argmax}_{r \in A_t} U_{ir,t} = j] = \frac{d_{j,t}^{\theta_{PA}} w_{ij}^{\theta_H} c_{ij,t}^{\theta_{TC}}}{\sum_{r \in A_t} d_{r,t}^{\theta_{PA}} w_{ir}^{\theta_H} c_{ir,t}^{\theta_{TC}}}.$$

Given a sequence of nodes $i_1, \dots, i_T \in V$ and choices (denoted by subscripted j) $j_1 \in A_1, \dots, j_T \in A_T$, the parameters can be found by maximizing the log-likelihood function. To get the standard errors of the coefficients and the corresponding P -values, we follow the process outlined in [40].

2.3.2 Experiment Setup and Rationale. We use datasets that refer to three US colleges – Caltech36, Swarthmore42, and UChicago30. They represent different sizes of networks: $n = 769$, $n = 1,659$, and $n = 6,591$ nodes, respectively.

For the Caltech36 ($n = 769$) and Swarthmore42 ($n = 1,659$) datasets, we consider all of the nodes of the networks as nodes that have to make a choice. For the UChicago30 dataset, we consider a randomly sampled subset of 2,000 nodes because of the limited context window of GPT models. We set the size of the alternative sets A_t to 20, and thus, the accuracy of random guessing is 5%.

2.3.3 Results. We present the regression results in Figure 5¹⁰. Our analysis reveals that the degree, the number of common neighbors, and the number of shared interests are all statistically significant factors influencing the choices of LLMs ($P < 0.001$) across all datasets. Furthermore, we find that LLMs place the greatest emphasis on the number of common attributes ($\hat{\theta}_H$), followed by the number of common neighbors ($\hat{\theta}_{TC}$), and then the degree ($\hat{\theta}_{PA}$).

⁹The standard Gumbel distribution has CDF $e^{-e^{-x}}$.

¹⁰More detailed results can be found in Table S.1 in Appendix A.

These results suggest that LLMs exhibit a strong preference for homophily, followed by a tendency towards triadic closure, and finally, preferential attachment. Specifically, the relationship $\hat{\theta}_H > \hat{\theta}_{TC} > \hat{\theta}_{PA}$ holds across all examined datasets and temperature settings.

In addition to the coefficient $\hat{\theta}_{TC}$ of triadic closure, we measure the percentage change in the average shortest path length and the average clustering coefficient between the network before the edge deletions and the network after the choices made by the LLM agents (see Table S.1). We observe that the average clustering coefficient also decreases compared to the initial network, indicating the weakening of triadic closure compared to the initial network.

We also provide reasoning analysis. Figure S.7 demonstrates that the rationales provided by LLMs aligns with the aforementioned findings. In particular, LLMs emphasize homophily, indicating that nodes sharing similar characteristics—such as student/faculty status, high school, and graduation year—are more likely to form connections. Conversely, the effects of triadic closure and preferential attachment are less prominent.

We also compare LLMs’ prediction with random guessing under a link prediction framework. We evaluate the percentage increase in accuracy, where accuracy is defined as the likelihood of selecting a previously existing neighbor from a set of alternatives, compared to making a random selection from 20 possible options. As shown in Appendix A, LLMs demonstrate a substantially higher accuracy in their selections than would be expected from random guessing.

Moreover, we examine whether the community structure is reinforced after the network formation decision made by LLMs. We run the Louvain algorithm 10 times for both the initial graph G_1 and the final graph G_T and perform a t-test between the resulting modularities (see Appendix A). We observe that the modularity increases in all cases and is statistically significant. This suggests that LLMs make choices that naturally yield a reinforcement of the community structure.

To reflect the relation with “small-world” phenomenon, we measure the percent change in the average shortest path length between the network before the edge deletions and the network after the choices made by the LLM agents (see Appendix A). We observe a small decrease in the average path length in the new network in almost all cases indicating that the average shortest path length decreases slightly, indicating strengthening of the small-world phenomenon.

Taken together, our analysis indicates that although preferential attachment, homophily, and triadic closure are all present in the network formation behaviors of LLMs, homophily emerges as the predominant driving force. Moreover, both community structure and small-world phenomenon are reinforced.

3 DISCUSSION

Our study conducted a comprehensive evaluation of LLMs’ network formation preferences, encompassing both micro-level network principles such as preferential attachment, triadic closure, and homophily and macro-level network principles like community structure and the small-world phenomenon. Our findings indicate that networks generated by multiple LLMs do exhibit these properties, particularly when primed with network statistics such as the number of mutual friends or the degree of alternatives. Furthermore, through discrete choice modeling, we explored the emergence of these properties in real-world networks. Our results reveal that the agents’ selections are predominantly driven by homophily, followed by triadic closure, and then preferential attachment. Additionally, we observed a strengthening of community structure in real-world network experiments.

Our study enhances our understanding of the behavior of multi-LLMs. For example, our findings reveal different strengths of network formation properties, suggesting that when LLMs are employed to coordinate social networks in social or work environments, they may exhibit behaviors similar

to humans. This insight contributes to developing socially aware LLMs that align with human preferences, with potential applications ranging from chatbots and virtual assistants to collaborative systems and social media platforms.

Furthermore, our study may pave the way for innovative applications of LLMs in network science research. Given that LLMs adhere to fundamental network principles and exhibit behaviors akin to human network formation, they hold significant potential for use in simulations of social systems and agent-based modeling. LLM agents have the capability to produce more sophisticated and nuanced behaviors, including negotiation, collaboration, and competition. This opens up opportunities to simulate networked environments such as marketplaces or organizational structures, where LLMs can model decision-making processes and interaction patterns.

Looking ahead, we propose three promising directions for future research. First, we propose investigating LLM behavior in more complex interactions, such as simulated dialogs or specific environments like companies, schools, or parties. By examining LLMs in these contexts, we can better understand their network formation preferences and how they adapt to different social dynamics. This research could shed light on the nuances of LLM behavior in realistic settings and inform their integration into diverse social environments. Second, we suggest exploring the application of our findings in specific settings, particularly in organizational contexts. For example, considering the potential use of LLMs to assist HR professionals, our study’s insights could guide the alignment of LLMs with organizational goals. By leveraging network information, LLMs could help HR departments identify their firms’ best fit or talent, optimizing recruitment and talent management processes. Finally, we propose using our methods to create realistic synthetic networks. These synthetic datasets can serve as benchmarks for evaluating graph learning methods, thus addressing the scarcity of existing graph benchmarks. By adjusting parameters like temperature, we can generate diverse networks to test graph neural network performance under various conditions. In addition, our approach can generate artificial data resembling real-world data while adhering to privacy regulations. This has the potential to expedite research in graph learning and trustworthy machine learning by providing realistic network datasets generated by LLMs.

4 METHODS

4.1 Experimental Procedure

In our study, we performed experiments to assess whether key network principles at both the micro-level (such as preferential attachment, triadic closure, and homophily) and the macro-level (including community structure and weak ties) align with classical network models. Subsequently, we utilized real-world networks to determine the factors that are most heavily weighted by LLMs.

Our experiments span a time series of T steps, with a sequence of network structures denoted as G_1, G_2, \dots, G_T . The initial network, G_1 , is referred to as the *seed network*. At each step t , we select a *query node* i_t (which may either be a new arrival or an existing node in the graph) and assign it the task of forming new links. This is accomplished by selecting nodes from a set of alternatives A_t (meaning potential candidates for link formation) and initiating a query call $Q(A_t, i_t, \delta)$ to the LLM (as outlined in Algorithm 1) to create up to δ new links. The edge set selection process involves presenting the LLMs with personal or network features of the alternatives, denoted as $F(A_t) = \{f_a : a \in A_t\}$, which may include information such as the neighbors of the nodes, node degrees, common connections with i_t , and community memberships, formatted in JSON. We adopt a zero-shot learning approach, avoiding the provision of examples to the model to prevent bias, in line with relevant studies such as [11]. This approach allows for the exploration of the innate preferences of LLMs.

We employ multiple temperatures to account for the variability in response generation by LLM systems, which is also observed in classical statistical models of network formation [23]. Our study conducts experiments using three temperatures: 0.5, 1.0, and 1.5.

Moreover, the model is tasked with outputting a JSON object indicating the node chosen for link formation and the rationale behind the choice. This approach is adopted because LLMs have demonstrated proficiency in processing code-like structures, such as HTML and JSON.

4.2 Summarizing the Reasoning of the LLM Agents

In addition to analyzing the innate preferences of LLM agents, we employ an interview-like approach to probe the rationale behind their decisions. Following the LLMs' decisions on network formation, we inquire about their reasoning for making those choices. We then aggregate all the provided rationales using GPT models (GPT-3.5 for Section 2.1 and GPT-4 for Section 2.3) by asking it to identify the common themes, resulting in the creation of multiple categories. To determine the category to which each LLM's reasoning belongs, we subsequently ask the GPT models to classify each rationale into the appropriate category.

4.3 Estimating the Parameters of the Discrete Choice Model

To estimate the parameters of the discrete choice model, we optimize the following log-likelihood function

$$(\hat{\theta}_{PA}, \hat{\theta}_{TC}, \hat{\theta}_H) = \arg \max_{(\theta_{PA}, \theta_{TC}, \theta_H) \in \mathbb{R}^3} \sum_{t=1}^T \left(\theta_{PA} \log d_{j_t, t} + \theta_H \log w_{i_t, j_t} + \theta_{TC} \log c_{i_t, j_t, t} - \log \left(\sum_{r \in A_t} d_{r, t}^{\theta_{PA}} w_{i_t, r}^{\theta_H} c_{i_t, r, t}^{\theta_{TC}} \right) \right),$$

where i_1, \dots, i_T are the chooser nodes (i.e., the LLM agents who want to form a link), and j_1, \dots, j_T are the nodes which are chosen from the alternative sets A_1, \dots, A_T . The likelihood function is convex, and we optimize it with the L-BFGS-B method [30]. The standard errors of the coefficients are approximated as $\sqrt{-H^{-1}}$ where H is the Hessian matrix of the log-likelihood at $(\hat{\theta}_{PA}, \hat{\theta}_{TC}, \hat{\theta}_H)$ (cf. [40, 48]).

ACKNOWLEDGMENTS

M.P. is supported by a scholarship from the Onassis Foundation (Scholarship ID: F ZT 056-1/2023-2024).

REFERENCES

- [1] Gati V Aher, Rosa I Arriaga, and Adam Tauman Kalai. 2023. Using large language models to simulate multiple humans and replicate human subject studies. In *International Conference on Machine Learning*. PMLR, 337–371.
- [2] Elif Akata, Lion Schulz, Julian Coda-Forno, Seong Joon Oh, Matthias Bethge, and Eric Schulz. 2023. Playing repeated games with Large Language Models. *arXiv preprint arXiv:2305.16867* (2023).
- [3] Eytan Bakshy, Itamar Rosenn, Cameron Marlow, and Lada Adamic. 2012. The role of social networks in information diffusion. In *Proceedings of the 21st international conference on World Wide Web*. 519–528.
- [4] Abhijit Banerjee, Arun G Chandrasekhar, Esther Duflo, and Matthew O Jackson. 2013. The diffusion of microfinance. *Science* 341, 6144 (2013), 1236498.
- [5] Albert-László Barabási. 2013. Network science. *Philosophical Transactions of the Royal Society A: Mathematical, Physical and Engineering Sciences* 371, 1987 (2013), 20120375.
- [6] Albert-László Barabási and Réka Albert. 1999. Emergence of scaling in random networks. *Science* 286, 5439 (1999), 509–512.
- [7] Ginestra Bianconi and A-L Barabási. 2001. Competition and multiscaling in evolving networks. *Europhysics letters* 54, 4 (2001), 436.
- [8] Vincent D Blondel, Jean-Loup Guillaume, Renaud Lambiotte, and Etienne Lefebvre. 2008. Fast unfolding of communities in large networks. *Journal of statistical mechanics: theory and experiment* 2008, 10 (2008), P10008.
- [9] Shikha Bordia and Samuel R Bowman. 2019. Identifying and reducing gender bias in word-level language models. *arXiv preprint arXiv:1904.03035* (2019).

- [10] Stephen P Borgatti and Martin G Everett. 2000. Models of core/periphery structures. *Social networks* 21, 4 (2000), 375–395.
- [11] Philip Brookins and Jason Matthew DeBacker. 2023. Playing games with GPT: What can we learn about a large language model from canonical strategic games? *Available at SSRN 4493398* (2023).
- [12] Yiting Chen, Tracy Xiao Liu, You Shan, and Songfa Zhong. 2023. The Emergence of Economic Rationality of GPT. *arXiv preprint arXiv:2305.12763* 120, 51 (2023), e2316205120. <https://doi.org/10.1073/pnas.2316205120> arXiv:<https://www.pnas.org/doi/pdf/10.1073/pnas.2316205120>
- [13] Felix Chopra and Ingar Haaland. 2023. Conducting qualitative interviews with AI. (2023).
- [14] Fan Chung and Linyuan Lu. 2004. The average distance in a random graph with given expected degrees. *Internet Mathematics* 1, 1 (2004), 91–113.
- [15] Aaron Clauset, Mark EJ Newman, and Cristopher Moore. 2004. Finding community structure in very large networks. *Physical review E* 70, 6 (2004), 066111.
- [16] Giordano De Marzo, Luciano Pietronero, and David Garcia. 2023. Emergence of Scale-Free Networks in Social Interactions among Large Language Models. *arXiv preprint arXiv:2312.06619* (2023).
- [17] Bahare Fatemi, Jonathan Halcrow, and Bryan Perozzi. 2023. Talk like a graph: Encoding graphs for large language models. *arXiv preprint arXiv:2310.04560* (2023).
- [18] James H Fowler and Nicholas A Christakis. 2008. Dynamic spread of happiness in a large social network: longitudinal analysis over 20 years in the Framingham Heart Study. *Bmj* 337 (2008).
- [19] Chen Gao, Xiaochong Lan, Zhihong Lu, Jinzhu Mao, Jinghua Piao, Huandong Wang, Depeng Jin, and Yong Li. 2023. S3: Social-network Simulation System with Large Language Model-Empowered Agents. *arXiv preprint arXiv:2307.14984* (2023).
- [20] Mark S Granovetter. 1973. The strength of weak ties. *American journal of sociology* 78, 6 (1973), 1360–1380.
- [21] James He, Felix Wallis, and Steve Rathje. 2023. Homophily in An Artificial Social Network of Agents Powered by Large Language Models. (2023).
- [22] John J Horton. 2023. *Large language models as simulated economic agents: What can we learn from homo silicus?* Technical Report. National Bureau of Economic Research.
- [23] Matthew O Jackson. 2008. *Social and economic networks*. Vol. 3. Princeton university press Princeton.
- [24] Abigail Z Jacobs and Duncan J Watts. 2021. A large-scale comparative study of informal social networks in firms. *Management Science* 67, 9 (2021), 5489–5509.
- [25] Eaman Jahani, Samuel P Fraiberger, Michael Bailey, and Dean Eckles. 2023. Long ties, disruptive life events, and economic prosperity. *Proceedings of the National Academy of Sciences* 120, 28 (2023), e2211062120.
- [26] Jon Kleinberg. 2000. The small-world phenomenon: An algorithmic perspective. In *Proceedings of the thirty-second annual ACM symposium on Theory of computing*. 163–170.
- [27] Hadas Kotek, Rikker Dockum, and David Sun. 2023. Gender bias and stereotypes in Large Language Models. In *Proceedings of The ACM Collective Intelligence Conference*. 12–24.
- [28] Yan Leng, Tara Sowrirajan, Yujia Zhai, and Alex Pentland. 2023. Interpretable stochastic block influence model: measuring social influence among homophilous communities. *IEEE Transactions on Knowledge and Data Engineering* (2023).
- [29] David Liben-Nowell and Jon Kleinberg. 2003. The link prediction problem for social networks. In *Proceedings of the twelfth international conference on Information and knowledge management*. 556–559.
- [30] Dong C Liu and Jorge Nocedal. 1989. On the limited memory BFGS method for large scale optimization. *Mathematical programming* 45, 1 (1989), 503–528.
- [31] Ding Lyu, Yuan Yuan, Lin Wang, Xiaofan Wang, and Alex Pentland. 2022. Investigating and modeling the dynamics of long ties. *Communications Physics* 5, 1 (2022), 87.
- [32] Benjamin S Manning, Kehang Zhu, and John J Horton. 2024. Automated Social Science: A Structural Causal Model-Based Approach. (2024).
- [33] Daniel McFadden. 1972. Conditional logit analysis of qualitative choice behavior. (1972).
- [34] Miller McPherson, Lynn Smith-Lovin, and James M Cook. 2001. Birds of a feather: Homophily in social networks. *Annual review of sociology* 27, 1 (2001), 415–444.
- [35] Mohsen Mosleh, Dean Eckles, and David Gertler Rand. 2024. *Tendencies toward triadic closure: Field-experimental evidence*. Technical Report. Center for Open Science.
- [36] Mark EJ Newman. 2003. Mixing patterns in networks. *Physical review E* 67, 2 (2003), 026126.
- [37] Mark EJ Newman. 2006. Modularity and community structure in networks. *Proceedings of the national academy of sciences* 103, 23 (2006), 8577–8582.
- [38] Mark EJ Newman and Michelle Girvan. 2004. Finding and evaluating community structure in networks. *Physical review E* 69, 2 (2004), 026113.
- [39] OpenAI. 2023. GPT-4 technical report. *arXiv* (2023), 2303–08774.

- [40] Jan Overgoor, Austin Benson, and Johan Ugander. 2019. Choosing to grow a graph: Modeling network formation as discrete choice. In *The World Wide Web Conference*. 1409–1420.
- [41] Marios Papachristou, Longqi Yang, and Chin-Chia Hsu. 2023. Leveraging Large Language Models for Collective Decision-Making. *arXiv preprint arXiv:2311.04928* (2023).
- [42] Joon Sung Park, Joseph C O’Brien, Carrie J Cai, Meredith Ringel Morris, Percy Liang, and Michael S Bernstein. 2023. Generative agents: Interactive simulacra of human behavior. *arXiv preprint arXiv:2304.03442* (2023), 1–22.
- [43] Patrick S Park, Joshua E Blumenstock, and Michael W Macy. 2018. The strength of long-range ties in population-scale social networks. *Science* 362, 6421 (2018), 1410–1413.
- [44] Bryan Perozzi, Bahare Fatemi, Dustin Zelle, Anton Tsitsulin, Mehran Kazemi, Rami Al-Rfou, and Jonathan Halcrow. 2024. Let Your Graph Do the Talking: Encoding Structured Data for LLMs. *arXiv preprint arXiv:2402.05862* (2024).
- [45] Iyad Rahwan, Manuel Cebrian, Nick Obradovich, Josh Bongard, Jean-François Bonnefon, Cynthia Breazeal, Jacob W Crandall, Nicholas A Christakis, Iain D Couzin, Matthew O Jackson, et al. 2019. Machine behaviour. *Nature* 568, 7753 (2019), 477–486.
- [46] E. M. Rogers. 2003. *Diffusion of Innovations* (5th ed.). Simon and Schuster.
- [47] Hugo Touvron, Louis Martin, Kevin Stone, Peter Albert, Amjad Almahairi, Yasmine Babaei, Nikolay Bashlykov, Soumya Batra, Prajjwal Bhargava, Shruiti Bhosale, Dan Bikel, Lukas Blecher, Cristian Canton Ferrer, Moya Chen, Guillem Cucurull, David Esiobu, Jude Fernandes, Jeremy Fu, Wenyin Fu, Brian Fuller, Cynthia Gao, Vedanuj Goswami, Naman Goyal, Anthony Hartshorn, Saghar Hosseini, Rui Hou, Hakan Inan, Marcin Kardas, Viktor Kerkez, Madian Khabsa, Isabel Kloumann, Artem Korenev, Punit Singh Koura, Marie-Anne Lachaux, Thibaut Lavril, Jenya Lee, Diana Liskovich, Yinghai Lu, Yuning Mao, Xavier Martinet, Todor Mihaylov, Pushkar Mishra, Igor Molybog, Yixin Nie, Andrew Poulton, Jeremy Reizenstein, Rashi Rungta, Kalyan Saladi, Alan Schelten, Silva Ruan, Smith Eric Michael, Subramanian Ranjan, Tan Xiaoqing Ellen, Tang Binh, Taylor Ross, Williams Adina, Xiang Jian, Xu Kuan Puxin, Yan Zheng, Zarov Iliyan, Zhang Yuchen, Fan Angela, Kambadur Melanie, Narang Sharan, Rodriguez Aurelien, Stojnic Robert, Edunov Sergey, and Scialom Thomas. 2023. Llama 2: Open Foundation and Fine-Tuned Chat Models. *arXiv preprint arXiv:2310.12345* (2023).
- [48] Kenneth E Train. 2009. *Discrete choice methods with simulation*. Cambridge university press.
- [49] Amanda L Traud, Peter J Mucha, and Mason A Porter. 2012. Social structure of facebook networks. *Physica A: Statistical Mechanics and its Applications* 391, 16 (2012), 4165–4180.
- [50] Veniamin Veselovsky, Manoel Horta Ribeiro, and Robert West. 2023. Artificial Artificial Artificial Intelligence: Crowd Workers Widely Use Large Language Models for Text Production Tasks. *arXiv:2306.07899* [cs.CL]
- [51] Jesse Vig, Sebastian Gehrmann, Yonatan Belinkov, Sharon Qian, Daniel Nevo, Yaron Singer, and Stuart Shieber. 2020. Investigating gender bias in language models using causal mediation analysis. *Advances in neural information processing systems* 33 (2020), 12388–12401.
- [52] Duncan J Watts and Steven H Strogatz. 1998. Collective dynamics of ‘small-world’ networks. *nature* 393, 6684 (1998), 440–442.
- [53] Yuan Yuan, Ahmad Alabdulkareem, and Alex ‘Sandy’ Pentland. 2018. An interpretable approach for social network formation among heterogeneous agents. *Nature communications* 9, 1 (2018), 4704.
- [54] Xuhui Zhou, Hao Zhu, Leena Mathur, Ruohong Zhang, Haofei Yu, Zhengyang Qi, Louis-Philippe Morency, Yonatan Bisk, Daniel Fried, Graham Neubig, et al. 2023. Sotopia: Interactive evaluation for social intelligence in language agents. *arXiv preprint arXiv:2310.11667* (2023).

A REGRESSION TABLE

In Table S.1, we report the regression coefficient for the regression in the real-world network data. The first column corresponds to the temperature, the next three columns correspond to the fitted coefficients from the regression model of Section 2.3 (also shown in Figure 5) accompanied by the standard errors (in parentheses) and the P -values indicated by stars (the null hypothesis corresponds to the parameters being set to 0). Next, LL corresponds to the log-likelihood of the fitted model, and AIC corresponds to the Akaike Information Criterion. Finally, we report the percent change in the accuracy compared to random guessing, the percent change in the average path length (as a measure of the small-world phenomenon), and the clustering coefficient (as a measure of the small-world phenomenon and the triadic closure), as well as the t -statistic for the change in modularity (Q) between the ground truth network dataset (before the edge deletions) and the network after the network formation process.

We observe that $\hat{\theta}_H > \hat{\theta}_{TC} > \hat{\theta}_{PA} > 0$ across all settings. LLM agents do better than random guessing, reinforce the small-world phenomenon, and weaken the triadic closure. Finally, the community structure is strengthened after new links are formed.

Temp.	$\hat{\theta}_{PA}$	$\hat{\theta}_H$	$\hat{\theta}_{TC}$	LL	AIC	% Change Acc.	% Change L	% Change C	ΔQ (t-stat)
Caltech36 (769 nodes, 33,312 edges)									
0.5	0.41*** (0.31)	1.95*** (0.64)	0.59*** (0.37)	-1,377.47	2,762.94	171.8	-0.008	-9.94	3.45**
1.0	0.36*** (0.13)	1.85*** (0.52)	0.58*** (0.33)	-1,435.07	2,878.13	179.6	-0.18	-11.08	3.49**
1.5	0.36*** (0.16)	1.72*** (0.31)	0.55*** (0.20)	-1,522.47	3,052.94	127.6	-0.06	-11.46	3.37**
Swarthmore42 (1,659 nodes, 12,2100 edges)									
0.5	0.18*** (0.13)	1.62*** (0.23)	0.65*** (0.08)	-2,838.33	5,684.66	124.2	0.01	-11.46	7.42***
1.0	0.26*** (0.07)	1.70*** (0.35)	0.58*** (0.12)	-2,927.99	5,863.97	91.6	-0.10	-4.25	1.96*
1.5	0.19*** (0.14)	1.50*** (0.33)	0.59*** (0.10)	-3,139.42	6,286.83	87.39	-0.20	-4.52	4.03***
UChicago30 (6,591 nodes, 416,206 edges)									
0.5	0.23*** (0.06)	2.00*** (0.24)	0.41*** (0.09)	-3,444.33	6,896.67	217.2	-0.24	-2.52	7.46*** [0.34]
1.0	0.23*** (0.10)	1.98*** (0.17)	0.38*** (0.06)	-3,578.18	7,164.36	219.2	-0.12	-2.66	9.56*** [1.05]
1.5	0.22*** (0.12)	1.78*** (0.27)	0.41*** (0.07)	-2,033.49	4,074.98	222.4	-0.17	-2.42	10.19*** [0.24]
Notes	$\hat{\theta}_{PA}$ = Coefficient of log degree, $\hat{\theta}_H$ = Coefficient of log # of common attributes, $\hat{\theta}_{TC}$ = Coefficient of log # common neighbors LL = Log-likelihood, AIC = Akaike Information Criterion Acc. = Accuracy, L = Average Path Length, C = Average Clustering Coefficient, ΔQ (t-stat) = Modularity change t-statistic * : $P < 0.05$, ** : $P < 0.01$, *** : $P < 0.001$								

Table S.1. Multinomial logit coefficients for three networks from the Facebook100 dataset. The standard errors of the estimates are shown in parentheses. The null hypothesis corresponds to the respective parameter being equal to 0. We report the percent change in accuracy, average path length, and average clustering coefficient compared to the initial network (before the deletion of edges). For the change in modularity, we run the Louvain algorithm ten times and perform a t-test with the resulting modularities. For the UChicago30 dataset, we report the t-statistic value in the subgraph induced by the 2,000 sampled nodes, since the newly added edges would have a very small effect on the change in the community structure if we were to measure it in the whole network. We also report the modularity change (t-statistic) of the whole graph inside brackets.

B ANALYTICAL REGRESSION TABLES

We present the regression tables for all the combinations of coefficients for each of the three real-world network datasets. For all datasets, we observe that $\hat{\theta}_{PA}$ is smaller than both $\hat{\theta}_{TC}$ and $\hat{\theta}_H$ in all models where any pair is included. Similarly, $\hat{\theta}_{TC}$ is always smaller than $\hat{\theta}_H$ in all models that are both included. Finally, note that whenever only $\hat{\theta}_{PA}$ and $\hat{\theta}_{TC}$ are considered, then $\hat{\theta}_{PA} < 0$ and the result is not statistically significant ($P > 0.05$).

Temp.	$\hat{\theta}_{PA}$	$\hat{\theta}_H$	$\hat{\theta}_{TC}$	Log Likelihood	AIC
0.5	0.50*** (0.04)			-2,236.36	4,476.71
0.5		2.78*** (0.07)		-1,511.42	3,026.85
0.5			1.53*** (0.04)	-1,506.01	3,016.02
0.5	0.64*** (0.06)	2.99*** (0.19)		-1,414.71	2,835.41
0.5	-0.02 (0.10)		1.53*** (0.08)	-1,505.95	3,017.90
0.5		1.43*** (0.11)	0.82*** (0.06)	-1,406.39	2,818.78
0.5	0.41*** (0.31)	1.95*** (0.64)	0.59*** (0.37)	-1,377.47	2,762.94
1.0	0.48*** (0.04)			-2,242.85	4,489.70
1.0		2.69*** (0.07)		-1,558.67	3,121.34
1.0			1.47*** (0.04)	-1,556.68	3,117.37
1.0	0.58*** (0.05)	2.86*** (0.08)		-1,473.13	2,952.26
1.0	-0.04 (0.06)		1.47*** (0.06)	-1,556.24	3,118.48
1.0		1.40*** (0.28)	0.79*** (0.06)	-1,457.76	2,921.52
1.0	0.36*** (0.13)	1.85*** (0.52)	0.58*** (0.33)	-1,435.07	2,878.13
1.5	0.50*** (0.04)			-2,233.25	4,470.50
1.5		2.51*** (0.07)		-1,646.83	3,297.65
1.5			1.36*** (0.04)	-1,636.20	3,276.40
1.5	0.57*** (0.07)	2.65*** (0.13)		-1,559.57	3,125.15
1.5	-0.01 (0.05)		1.37*** (0.04)	-1,636.19	3,278.37
1.5		1.29*** (0.11)	0.75*** (0.06)	-1,546.78	3,099.55
1.5	0.36*** (0.16)	1.72*** (0.31)	0.55*** (0.20)	-1,522.47	3,052.94

Note * : $P < 0.05$, ** : $P < 0.01$, *** : $P < 0.001$

Table S.2. Multinomial logit coefficients for Caltech36. The standard errors of the estimates are shown in parentheses.

Temp.	$\hat{\theta}_{PA}$	$\hat{\theta}_H$	$\hat{\theta}_{TC}$	Log Likelihood	AIC
0.5	0.33*** (0.03)			-4,978.28	9,960.56
0.5		2.91*** (0.05)		-3,027.03	6,058.06
0.5			1.37*** (0.02)	-3,014.28	6,032.57
0.5	0.44*** (0.15)	2.99*** (0.10)		-2,948.91	5,903.82
0.5	-0.18*** (0.09)		1.36*** (0.07)	-3,002.17	6,010.35
0.5		1.42*** (0.11)	0.72*** (0.07)	-2,847.16	5,700.32
0.5	0.18*** (0.13)	1.62*** (0.23)	0.65*** (0.08)	-2,838.33	5,684.66
1.0	0.38*** (0.03)			-4,959.02	9,922.04
1.0		2.83*** (0.05)		-3,119.06	6,242.11
1.0			1.32*** (0.02)	-3,118.13	6,240.26
1.0	0.50*** (0.16)	2.92*** (0.09)		-3,018.85	6,043.71
1.0	-0.11** (0.09)		1.32*** (0.07)	-3,113.21	6,232.43
1.0		1.41*** (0.15)	0.69*** (0.11)	-2,947.89	5,901.78
1.0	0.26*** (0.07)	1.70*** (0.35)	0.58*** (0.12)	-2,927.99	5,863.97
1.5	0.36*** (0.03)			-4,952.51	9,909.02
1.5		2.64*** (0.05)		-3,324.71	6,653.43
1.5			1.24*** (0.02)	-3,306.06	6,616.11
1.5	0.44*** (0.11)	2.71*** (0.05)		-3,241.67	6,489.35
1.5	-0.14*** (0.10)		1.24*** (0.05)	-3,298.07	6,602.13
1.5		1.30*** (0.14)	0.67*** (0.09)	-3,150.29	6,306.57
1.5	0.19*** (0.14)	1.50*** (0.33)	0.59*** (0.10)	-3,139.42	6,286.83

Note * : $P < 0.05$, ** : $P < 0.01$, *** : $P < 0.001$

Table S.3. Multinomial logit coefficients for Swarthmore42. The standard errors of the estimates are shown in parentheses.

Temp.	$\hat{\theta}_{PA}$	$\hat{\theta}_H$	$\hat{\theta}_{TC}$	Log Likelihood	AIC
0.5	0.28*** (0.02)			-5,983.56	11,971.13
0.5		2.93*** (0.05)		-3,637.18	7,278.37
0.5			1.11*** (0.02)	-3,740.78	7,485.55
0.5	0.38*** (0.04)	3.06*** (0.21)		-3,523.06	7,052.12
0.5	-0.04 (0.08)		1.11*** (0.04)	-3,739.31	7,484.61
0.5		1.68*** (0.13)	0.51*** (0.07)	-3,477.37	6,960.75
0.5	0.23*** (0.06)	2.00*** (0.24)	0.41*** (0.09)	-3,444.33	6,896.67
1.0	0.28*** (0.02)			-5,982.66	11,969.32
1.0		2.85*** (0.05)		-3,759.78	7,523.56
1.0			1.07*** (0.02)	-3,879.04	7,762.08
1.0	0.36*** (0.07)	2.96*** (0.31)		-3,649.84	7,305.68
1.0	-0.04 (0.06)		1.07*** (0.03)	-3,877.83	7,761.66
1.0		1.67*** (0.11)	0.49*** (0.08)	-3,611.48	7,228.95
1.0	0.23*** (0.10)	1.98*** (0.17)	0.38*** (0.06)	-3,578.18	7,164.36
1.5	0.30*** (0.03)			-3,241.67	6,487.34
1.5		2.71*** (0.06)		-2,145.02	4,294.03
1.5			1.03*** (0.02)	-2,175.32	4,354.64
1.5	0.37*** (0.08)	2.81*** (0.10)		-2,080.67	4,167.34
1.5	-0.01 (0.04)		1.03*** (0.04)	-2,175.25	4,356.49
1.5		1.50*** (0.10)	0.51*** (0.04)	-2,051.61	4,109.23
1.5	0.22*** (0.12)	1.78*** (0.27)	0.41*** (0.07)	-2,033.49	4,074.98
Note				* : $P < 0.05$, ** : $P < 0.01$, *** : $P < 0.001$	

Table S.4. Multinomial logit coefficients for UChicago30. The standard errors of the estimates are shown in parentheses.

C LLM REASONING SUMMARIZATION

In addition to studying LLM agents’ innate preferences, we use an interview-style approach to understand why they make certain decisions. After LLMs form networks, we ask them about their reasoning. We then use GPT models (GPT-3.5 for Section 2.1 and GPT-4 for Section 2.3) to group their explanations into common themes, creating various categories. To classify each LLM’s reasoning, we have the GPT models assign them to the relevant category.

C.1 Micro-level Principles

In Figure S.6, we show the reasoning of the LLM agents from the networks of Section 2.1.

In Figures 6(a) and 6(b), the reasons mean the following:

- *Well-Connectedness*: it corresponds to reasons related to the person being well-connected and having many friends.
- *Mutual Friends*: it is related to having many friends in common with the person so that the person can introduce them to their friends.

We observe that for Figure 6(a), the well-connectedness reason becomes less important as the temperature increases while having more mutual friends becomes more important as the temperature increases. This means that the agents emphasize triadic closure in higher temperatures and decrease emphasis on preferential attachment. For Figure 6(b), we observe an opposite pattern in the LLM reasoning. A possible explanation for this asymmetry is the fact that different types of features are provided, i.e., in the case of Figure 6(a) the neighbors of each node are provided, whereas in the case of Figure 6(b) the common neighbors with the query node i_t are provided.

Finally, Figure 6(c) contains the reasons for Figure 3(a) based on having a common hobby, a common color, or a common location. We observe that the LLM agents make choices primarily based on sharing the same hobby and then based on a common location or a common color (on an almost equal basis).

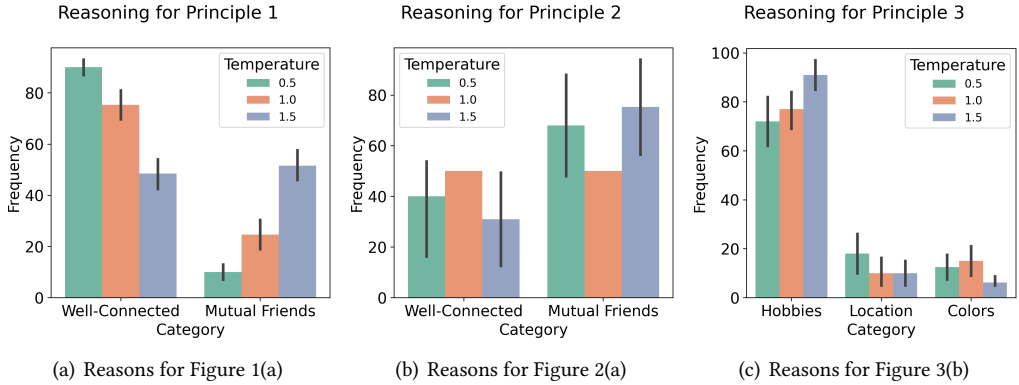


Fig. S.6. Distribution of reasoning across categories for the networks of Figures 1(a), 2(a) and 3(b). The classification uses GPT-3.5 on 20 randomly sampled reasons repeated over five times (micro-averaged frequencies). The error bars correspond to 95% confidence intervals.

C.2 Real-world Data

We also present the LLM reasoning for real-world networks. The reasons have been set so that there is a one-to-one correspondence with the regression coefficients. Specifically, the *Mutual Friends* reason corresponds to $\hat{\theta}_{TC}$, the *Number of friends* reason to $\hat{\theta}_{PA}$, and the *Similar attributes* reason corresponds to $\hat{\theta}_H$ respectively. Consistently with the results reported in Table S.1, the agents' reasoning is more geared towards homophily (same attributes), then triadic closure (mutual friends), and finally preferential attachment (number of friends). These results are consistent with the regression.

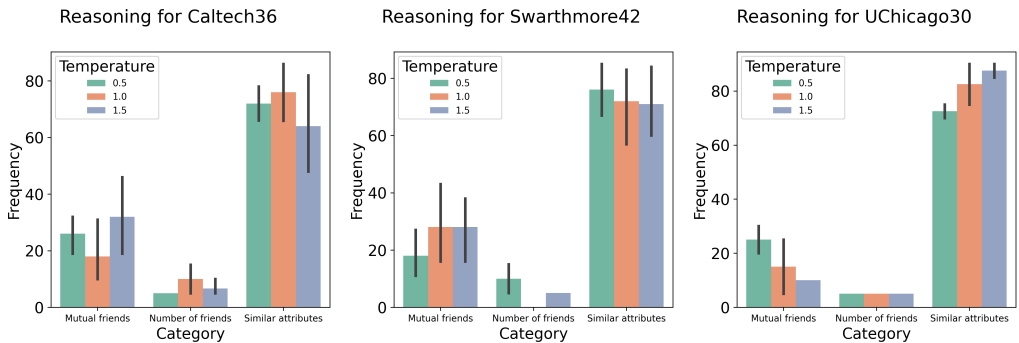


Fig. S.7. Distribution of reasoning across categories for the real-world networks. The classification is done using GPT-4 on a set of 20 randomly sampled reasons repeated over 5 times. In agreement with Table S.1, the multi-LLMs put more weight on homophily, then on triadic closure, and then on preferential attachment. The error bars correspond to 95% confidence intervals.

D NETWORK EVOLUTION

Here we depict the evolution of the networks generated by the LLM agents.

D.1 Principle 1: Preferential Attachment

We plot the evolution of the LLM-based preferential attachment networks at three timesteps, together with the degree distribution alongside the degree distribution of a BA graph with the same number of nodes. We observe that for the temperature being 0.5 we have a core-periphery like formation which diverges from the BA model, whereas for the temperature being 1.5 the network has the same degree distribution as the BA model.

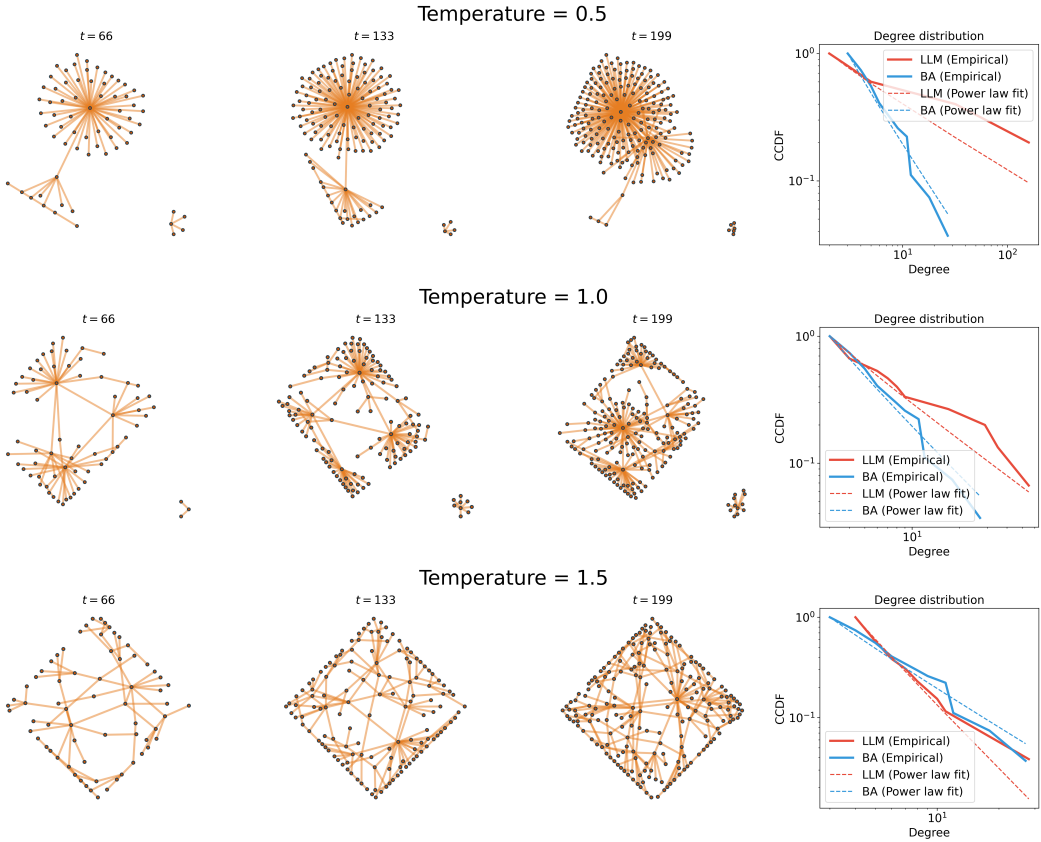


Fig. S.8. Dynamic evolution of networks created based on Principle 1.

D.2 Principle 2: Triadic Closure

We plot the evolution of the LLM-generated networks based on the triadic closure principle, together with the transitivity measure and the algebraic connectivity (which corresponds to the second-smallest eigenvalue of the graph Laplacian). We observe that the algebraic connectivity gradually increases as new edges between the clusters are created. Specifically, the algebraic connectivity reaches a higher value for higher temperatures, indicating the more frequent creation of new intra-cluster edges. Moreover, we observe that the transitivity initially increases and then decreases until it reaches its final value.

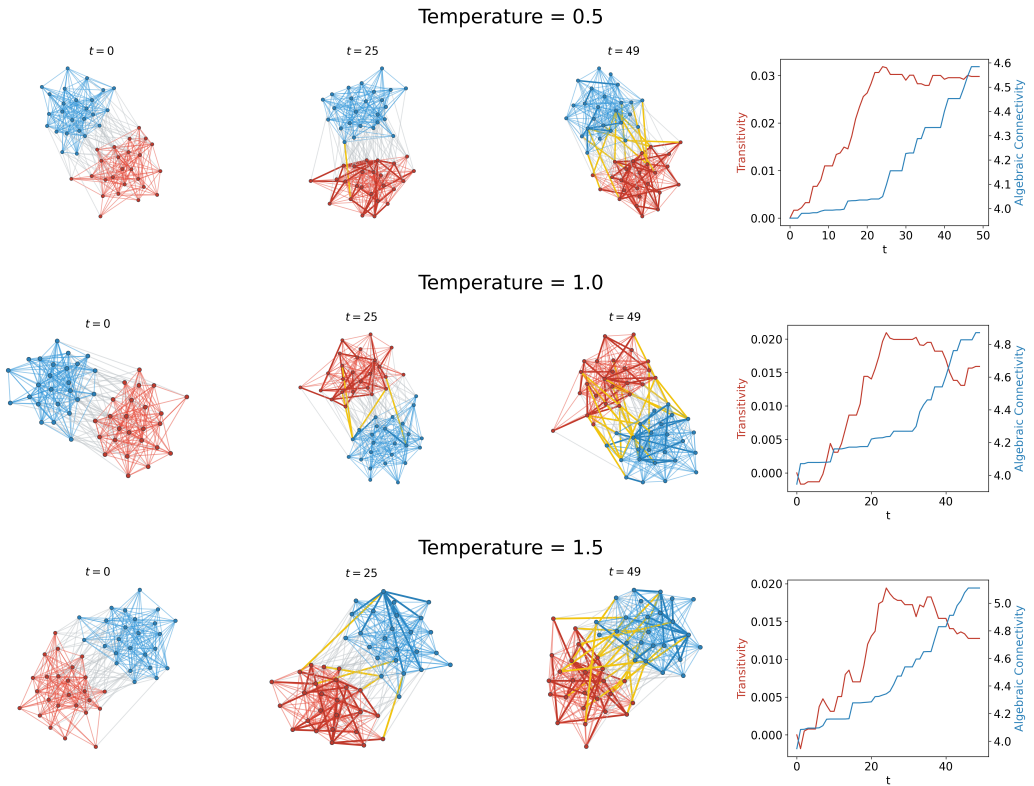


Fig. S.9. Dynamic evolution of networks created based on Principle 2.

E FEATURE REPRESENTATIONS FOR PROMPTS

Below, we give examples of the features used in the prompt presented in Algorithm 1. The features are formatted as a list of JSON objects which are provided to the prompt.

E.1 Principle 1: Preferential Attachment

For the structure-based information (Figure 1(a)) we have the following features:

```
[
  {
    "name" : 0,
    "neighbors" : [5, 7, 1, 6]
  },
  ...
]
```

And for the degree-based information (Figure 1(b)) we have the following features:

```
[
  {
    "name" : 0,
    "degree" : 4
  },
  ...
]
```

E.2 Principle 2: Triadic Closure

For the structure-based information (Figure 2(a)) we have the following features:

```
[
  {
    "name" : 0,
    "common_neighbors" : [5, 7, 1, 6]
  },
  ...
]
```

And for the degree-based information (Figure 2(b)) we have the following features:

```
[
  {
    "name" : 0,
    "num_common_neighbors" : 4
  },
  ...
]
```

E.3 Principle 3: Homophily

We have the following features:

```
[
  {
    "name" : 0,
    "favorite_color" : "red",
    "hobby" : "hiking",
    "location" : "Boston"
  },
  ...
]
```

E.4 Principle 5: Small-World

We have the following features:

```
[
  {
    "name" : 0,
    "neighbors" : [5, 7, 1, 6]
  },
  ...
]
```

E.5 Real-World Data

We have the following features:

```
[
  {
    "name" : 0,
    "status" : "student",
    "major" : 10,
    "second major" : 93,
    "accommodation" : "house",
    "high_school" : 5,
    "graduation_year" : 2008
  },
  ...
]
```

We note that the initial Facebook100 dataset included gender information as a feature. We chose not to include the gender as one of the features as it has been shown that language models exhibit gender bias [9, 27, 51].